Journal of Materials Chemistry A

Molecular dynamics simulation of strong interaction mechanisms at wet interfaces in clay-polysaccharide nanocomposites

Journal:	*Journal of Materials Chemistry A*
Manuscript ID:	TA-ART-03-2014-001459.R1
Article Type:	Paper
Date Submitted by the Author:	24-Apr-2014

Complete List of Authors:	Wang, Yan; Royal Institute of Technology, Theoretical Chemistry and Biology Wohlert, Jakob; KTH Royal Institute of Technology, Wallenberg Wood Science Center Berglund, Lars; Royal Inst of Technology, Wallenberg Wood Science Center Tu, Yaoquan; Royal Institute of Technology, Theoretical Chemistry and Biology Agren, Hans; KTH Royal Institute of TechnologyN, Division of Theoretical Chemistry and Biology, School of Biotechnology

Journal of Materials Chemistry A RSCPublishing

ARTICLE

Molecular dynamics simulation of strong interaction mechanisms at wet interfaces in clay-polysaccharide nanocomposites

Cite this: DOI: 10.1039/x0xx00000x

Received x x th x x x x 2014,
Accepted x x th x x x x 2014

DOI: 10.1039/x0xx00000x

www.rsc.org/

Yan Wang,[a] Jakob Wohlert,*[bc] Lars A. Berglund,[bc] Yaoquan Tu,[a] and Hans Ågren*[a]

Bio-composites comprised of the polysaccharide xyloglucan (XG) and montmorillonite (MTM) clay has potential as a 'green' replacement of conventional petroleum-derived polymers in the packaging industry. These materials have been shown to possess excellent material properties, even in high relative humidity. Although interfacial interaction between XG and MTM, and the molecular structure of XG can be identified as key parameters for the complex formation process and the resulting tensile properties, these properties are usually difficult to address using experimental methods. Here we use molecular dynamics (MD) simulations to study the adsorption of fully atomistic models of both native and chemically modified XG to MTM clay surfaces in explicit water. We show that the driving force for adsorption is a favorable change in enthalpy, and furthermore that native XG adsorbs stronger than modified XG. This highlights the importance of molecular structure details to molecular adhesion. The present study provides insights into the molecular scale adsorption mechanisms and can therefore help in designing routes for further improvements of bio-composite materials.

1 Introduction

In nature, most load-bearing materials are nanostructured composites. Several contain inorganic particles and examples such as bone, dentin and nacre have sophisticated nanoscale organization[1]. Biological materials are usually highly hydrated, and yet have substantial mechanical function. In contrast, man-made biocomposites can show severe property degradation in high humidity or wet environments[2]. The main reason for this difference in properties is that in biological materials, molecular scale interfacial adhesion between reinforcement and matrix phase is also high in the hydrated state. In order to improve the characteristics of man-made nanocomposites in this respect, it is of interest to study bio-inspired composites both experimentally and theoretically. "Processing" of biological composites takes place at ambient temperature and with water rather than organic solvents as liquid medium. Improved understanding of the hydrated state in biocomposites is therefore one objective in the present study. Biological composites are also based on just a few simple building blocks, where unique properties are obtained through molecular and nanostructural control[3]. This control is often based on self-assembly mechanisms, which have been difficult to mimic. For the case of nacre, the work by Tang et al. [4] on nanostructured artificial nacre was therefore a breakthrough, where the layered and parallel orientation of inorganic platelets in nacre ("brick and mortar" structure) was mimicked, The study showed that it was possible to reach high inorganic content (volume fraction $\approx$ 50%), a modulus of 11 GPa and a tensile strength of 100 MPa. Furthermore, MTM clay platelets were combined with a charged, water-soluble polymer in a layer-by-layer process. However, in moist condition the mechanical properties were strongly degraded. It is likely that water molecules reduced MTM-polymer interactions at the interface, which contributed to degradation of properties. In contrast, two recent experimental studies of oriented MTM-polysaccharide nanocomposites demonstrated unexpectedly good preservation of mechanical and barrier properties in the moist state[5, 6]. The polysaccharide used was xyloglucan (XG), a high molar mass hemicellulose obtained from tamarind seed waste [7]. It was further noted that removal of galactose side groups from XG reduced adhesion with MTM.[5]

Xyloglucan is widely studied due to its importance in linking cellulose microfibrils in the hydrated primary cell wall of plants. The linking takes place by physical adsorption of XG to cellulose. Experimental studies of XG adsorption to cellulose[8] are of apparent importance. One advantage with complementary molecular dynamics (MD) simulations of experimentally studied materials is that the fundamental thermodynamics can be analyzed. Changes in free energy can be related to complex molecular-level processes, and also decomposed into changes in enthalpy and entropy. This has been demonstrated for adsorption of XG to cellulose in water[9], and is an important motivation for the present study. Focus is on MTM-XG where the interfacial adhesion in the presence of water is unexpectedly well preserved [5].

The present study employs a simple model of an MTM-XG interface, containing one layer of MTM and one single chain of XG. MD simulations were used in order to investigate the adsorption process and the conformational properties of XG in explicit water. In the present model, two model oligosaccharides were used to represent native xyloglucan (Native XG) and an enzymatically modified XG (Modified XG) (see Fig. 1). Each XG fragment was interacting with a single layer of MTM and adsorption behavior, as well as work of adhesion, of the two different XG fragments were compared. The free energy of pulling XG off the MTM surface was calculated from potentials of mean force (PMF), and the conformational entropy of XG was estimated using a quasiharmonic (QH) analysis. The study contributes to a better understanding of materials design principles for moisture-stable clay nanocomposites.

2 Methods

2.1 The model

In this study a simplified model of native XG was set up by linking two oligosaccharide units, XXLG and XXXG (Fig 1 (a)). Further, a ninth glucose unit was linked to the non-reducing end of the backbone to reduce the chain-end effects.[9] In total, this corresponds to a molecular weight of 2.9 kDa. This is certainly much lower than for real, native XG, which usually has a molecular weight of the order MDa. However, recent experimental data shows that XG with as low molecular weight as 4 kDa also adsorbs to MTM clay, albeit to a little less extent than native XG due to its increased aqueous solubility. Inspired by the experimental work of Kochumalayil et al.[5], where the extent of galactose removal was around 40% using β-galactosidase,[5] a simplified model for a modified XG was created by changing the L residue into an X (see Fig. 1 (b)). Thus, the two model XG fragments differ only in the composition of one of their side chains, and the effect on MTM-XG interaction will be studied.

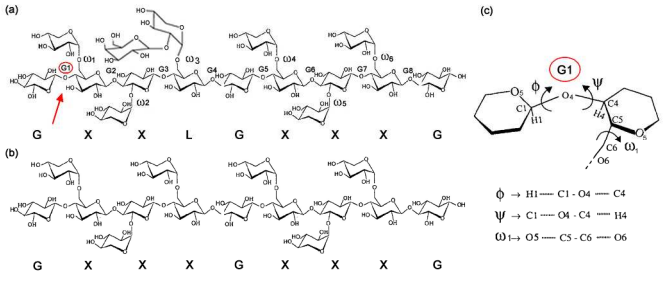

Figure. 1 Model of the two XGs: (a) Sequence of a native XG specified as GXXLGXXXG, with G1 to G8 describing the glycosidic linkage and ω1 to ω6 the side chain conformations; Here, G denotes an unsubstituted β-D-Glcp unit, X an β-D-Xylp-(1-6)- β-D-Glcp-(1-4) unit and L an β-D(1-2)-Galp(1-2)- α-D-Xylp-(1-6)- β-D-Glcp-(1-4) unit; (b) Sequence of the modified XG specified as GXXXGXXXG; (c) Definition of the dihedral angles in glycosidic linkages and side chains. [10]

The initial conformations of the XG fragments were built using the Amber Leap module[11], according to the work of Levy[10] in which the dihedral angles were determined to match the global minimum structures. In addition, the initial backbone was twisted with (Φ, Ψ) = (56°, 3°) and with the side chains arranged like a helix with respect to the central backbone axis. The definition of the dihedral angles Φ, Ψ and ω is shown in Fig. 1 (c). The size of the XGs can be found in Table 1.

System	No. of Atoms	No. of Water molecules	No. of XGs atoms	Size of XGs (nm^3)	No. of Counter ions (Na^+)	System size (nm^3)
Native XG-MTM	56310	16220	315	1.5×4.7×1.4	135	9.3×9.0×6.9
Modified XG-MTM	56856	16409	294	1.3×4.7×1.3	135	9.3×9.0×6.9

Table 1. Size of the simulation boxes for the XG-MTM systems.

In the present work, the MTM model was created according to the MTM composition of a sodium smectite clay[12], where the dioctahedral structure was based on the structure of pyrophyllite[13]. An overall neutral super-cell consisting of four unit MTM clay cells and three sodium counter ions $(Na_3(Si_{31}Al)(Al_{14}Mg_2)O_{80}(OH)_{16} \bullet 16H_2O)$[14] was used. It was replicated laterally along the X and Y axis to produce large enough surface to interact with XG fragments in different starting orientations with minimal edge effects. The simulation systems are listed in Table 1.

To start the simulations, each XG fragment was placed parallel to the MTM surface with its center of mass at a distance of 1.2-1.5 nm above the surface (See Fig.2 (a)). Two main orientations were considered: one perpendicular to the direction [100] (called A [0°] here) and one parallel to the direction of [100] (called B [0°]) (See Fig. 2(b), (c)). Six other orientations, corresponding to A [90°], A [180°], A [270°] and B [90°], B [180°], B [270°] were generated by rotating the XG along the direction of its backbone clockwise. In this way, eight initial structures were generated. Thereafter, each system was put in a rectangular box and a number of water molecules that varied between 16220 and 16409 were added. To keep the overall system neutral, 135 sodium counter ions were added to the simulation box. Fig. 2 illustrates the initial structure of the XG-MTM system with the definition of A and B orientations, prior to starting the MD simulations.

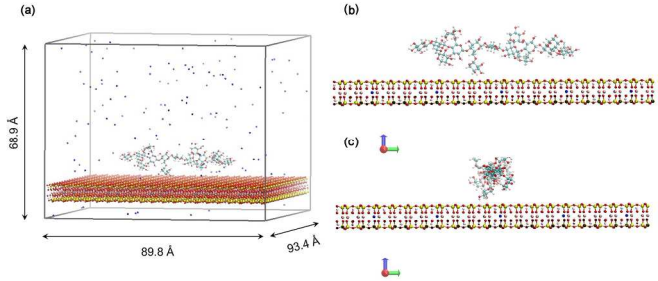

Figure 2. Starting structure of the XG-MTM system model and the definition of the XG orientations of the starting conformation; (a) the visualization depicts the tetrahedral and octahedral layers of the clay, the exposed surface, as well as the XG conformation chains in the initial simulation box; (b) define the orientation as A[0°] and (c) define the orientation as B[0°], six other orientations (A[90°],

A[180°], A[270°], B[90°], B[180°], B[270°]) were generated by rotating XG along the backbone clockwise by 90°. Color scheme is as follows: O (red), H (white), C (cyan), Si (yellow), Al (pink), Na (light blue), Mg (dark blue), X axis (red), Y axis (green), Z axis (blue). Water molecules are not shown.

2.2 Computational details

The molecular dynamics (MD) simulation technique implemented in the GROMACS 4.5.5 package was applied to simulate all systems.[15, 16] Generally, it is difficult to describe interactions between inorganic minerals and organic molecules with just one single molecular mechanics force-field, since most force-fields are parameterized for some specific system. GLYCAM06 is a general-purpose force field for carbohydrates [17] that has been shown to work well for XG before [9]. At the same time, CLAYFF is a suitable choice for simulations of hydrated, multi component mineral system and their interfaces with aqueous solutions [14]. More importantly, both GLYCAM06 and CLAYFF use the same protocol for defining partial atomic charges, which makes it possible to obtain reasonable electrostatic interactions when they are mixed. Previous simulations carried out on DNA-intercalated layered double hydroxides demonstrated a successful combination of the Amber f99 force field with ClayFF.[18] They applied Lorentz-Berthelot mixing rules for the Lennard-Jones parameters. It was concluded that this approach would work well for the case when the electrostatic interactions dominate the potential energy.[18] The same mixing rules thereby were used here. Water molecules were represented using the simple point charge (SPC) model of Berendsen et al.[19] Periodic boundary conditions were applied in all directions. The MD simulation details can be found in Supporting Information (SI).

Free energy profiles of pulling the XG fragments off the MTM surface were calculated from the potential of mean force (PMF) using umbrella sampling[20]. The configurational part of the entropy change for the same process was estimated using a quasiharmonic (QH) analysis [21] with corrections [22]. A detailed description of these methods can be found in SI.

3 Results and discussion

3.1 XG-MTM interaction energy in the adsorbed state

For each XG in 8 different orientations, a total of 16 systems with 100ns of dynamics were run. After approximately 80 ns the systems reached the equilibrium, since both the instantaneous interaction energy between the XG and the MTM (excluding water and counter ions), as well as the root-mean-square deviation (RMSD) of the XG were stabilized (See Eqns. (1) and (2) Fig. (S1) and Fig. (S2) in SI).

To investigate if the adsorption behavior of the XGs on the MTM surface are sensitive to the initial orientations, the interaction energy for all the eight systems for each XG with different starting conformations are given in Fig. 3. The results show that the two XG fragments were adsorbing onto the MTM surface regardless of orientation, however, with a slight preference of the B orientation (parallel to the direction of [100]). Out of eight orientations studied, the B [180°] orientation exhibited the lowest interaction energy (strong interaction) for both fragments. For each XG fragment, the interaction energy averaged over all eight orientations is summarized in Table 2, here the separate contributions from electrostatic interaction energy (E_{coul}) and the van der Waals interaction energy (E_{vdw}) are also listed. Electrostatics dominates the interaction between XG and MTM, on average accounting for about 60% of the total interaction energy, for both native and modified XG.

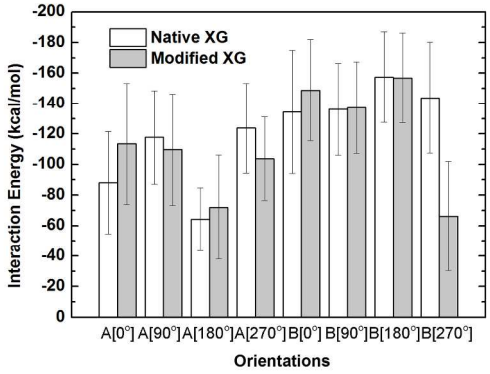

Figure 3. The interaction energy between each XG fragment and MTM for eight different orientations, averaged over the last 20 ns of the simulation data.

Table 2. XG-MTM averaged interaction energies.

XGs	[a]ΔE_{int} (A)	[b]ΔE_{int} (B)	[c]ΔE_{int} (total)	[d]ΔE_{coul}	[e]ΔE_{vdw}
Native XG	-98.5	-143.0	-120.7	-72.4	-47.7
Modified XG	-99.8	-127.3	-113.5	-66.8	-47.2

[a] Interaction energy averaged over four A orientations; [b] Interaction energy averaged over four B orientations; [c] Interaction energy averaged over the total eight different orientations; [d] The electrostatic part of the interaction energy averaged over all eight different orientations; [e] The van der Waals part of the interaction energy averaged over all eight different orientations. All the data were based on the last 20 ns of the trajectories. The energy unit is kcal/mol.

3.2 Binding affinity at the XG-MTM interface

For macroscopic materials, interfacial adhesion in the presence of water is critical. In this context, the interaction mechanisms at the XG-MTM interface are of great interest. One way to study adsorption capability is to calculate the free energy profile pertaining to the desorption process. Here, the potential of mean force (PMF) was calculated by reversibly pulling the two XG fragments off the MTM surface into the water phase, starting from their respective lowest energy state (See Fig. 4 and SI). The perpendicular distance from the MTM surface to the centre of mass of the XG was used as reaction coordinate, ξ, with ξ=0 meaning the state where the XG was fully adsorbed.

From the PMFs the desorption free energy ΔG was estimated. It was calculated as the free energy difference between the global minimum and the plateau value. It turned out to be higher for native MTM-XG than for modified, 27 kcal/mol and 23 kcal/mol, respectively. Nevertheless, both variants exhibit a clear affinity for MTM in the presence of water. This is quite remarkable, and one of the central findings of this study, since it shows why the properties of composite materials made from XG and MTM clay, to a surprisingly large extent, do not degrade in moist conditions.

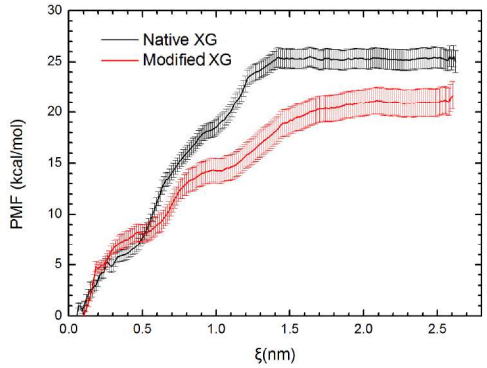

Figure 4. Free energy profiles of the native XG-MTM (black line) and modified XG-MTM (red line) with the statistical error bars, ξ=0 is the fully adsorbed state, corresponding to the free energy minimum of the detaching process.

It is also interesting to note that the modified XG has lower affinity to MTM than the native one, also when the numbers are corrected for their difference in mass. This is despite the fact that removal of side groups makes the polymer less flexible, which will favor the adsorbed state for entropy reasons. This also correlates with the experimental observation that native XG exhibits stronger binding affinity to MTM.[5] The authors of that study speculate that reason for this is that modified XG has better packing than the native one, leading to an increased propensity to form aggregates in solution. This would consequently reduce adsorption. However, the present study shows that the difference can also be due to that native XG form stronger direct interactions with the MTM surface.

To put these numbers into perspective, one can compare them to the previous study of XG adsorption on a crystalline cellulose surface, where the affinity was computed to 34.5 kcal/mol for GXXLGXXXG (native XG here) and 31.4 kcal/mol for GXXXGXXXG (modified XG).[9] This is certainly higher than the values computed here, but that is perhaps not so surprising considering the role of XG plays in the plant cell wall.

It may also be interesting to transform these numbers into work of adhesions, W_A, which are experimentally available for many systems, although not for this particular one. The work of adhesion between two phases is defined as the free energy per unit interfacial area, and if one assumes an area per sugar residue of 0.5 times 0.5 nm^2, one gets W_A = 0.6 – 0.7 J/m^2, which falls in the range one expects for ideal molecular systems that are not affected by macroscopic effects like surface roughness or contaminants [23].

3.3 Decomposition of the free energy

The entropy and the enthalpy (potential energy) contributions to the desorption free energies were analyzed separately. This facilitates an understanding of the thermodynamic driving forces. In particular, the role of water for the binding affinity is of interest.

3.3.1 Potential energy.

The total potential energy change of the whole system, ΔU, was recorded as a function of separation (see Fig. 5). Due to large fluctuations in U (originating mainly from water/water interactions) it is not possible to give a very precise value, or even to discriminate between the native XG and modified XG fragments. It is however possible to give a rough estimate of ΔU somewhat in the range 15 - 25 kcal/mol. Thus, it seems as if the major part of ΔG is accounted for by ΔU. Since ΔG = ΔU – TΔS, this has the implication that ΔS, which is the change in entropy for the process, has to be close to zero.

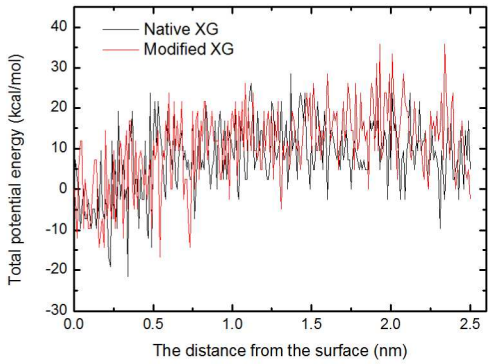

Figure 5. The total potential energy relative the adsorbed state, as a function of the distance from the surface during the desorption process. Black line represents the contribution from the native XG fragment and red line represents that from the modified one.

3.3.2 Entropy.

The entropy change ΔS for the desorption process can be assumed to mainly consist of two terms: ΔS_{SOL} and ΔS_{XG} which are the entropy changes for the water solution (including counter ions), and the XG fragment, respectively. This assumes that these contributions can be separated, and also that the entropy change of the MMT is negligible. Here, ΔS_{XG} was estimated from a quasiharmonic (QH) analysis, including corrections for anharmonicity and correlations between eigenmodes, of 60 ns long simulations of the adsorbed and the free state, respectively, which gives the absolute configurational entropy in each state. [21, 22]

The configurational entropy of the XG fragments was calculated to approximately 1 kcal/mol/K for the adsorbed states, and a little higher, 1.2-1.3 kcal/mol/K for the free fragment in solution (see Table 3). The correction term accounting for the anharmonicity of the eigenmodes, ΔS_{ah}, is small in all cases, whereas the term correcting for pair-wise correlations between the modes, ΔS_{pc}, is much larger, and definitely non-negligible. This has been noted before in the case of proteins in water[22, 24], but also for carbohydrates in aqueous solution[25, 26]. The total entropy change upon desorption, including corrections, is 0.2 and 0.3 kcal/mol/K for the modified and the native XG respectively (see Table 3). That the value for modified XG is smaller makes sense considering the reduced number of degrees of freedom of that fragment.

Table 3. Quasiharmonic entropies and correction terms for both native and modified XG fragments in the adsorbed and the free states respectively.

States	Entropy term	Native XG	Modified XG
Adsorbed	S_{QH}	1.026	1.059
	ΔS_{ah}	-0.002	-0.002
	ΔS_{pc}	-0.012	-0.034
Free	S_{QH}	1.360	1.242
	ΔS_{ah}	-0.002	-0.002
	ΔS_{pc}	-0.086	-0.060
	ΔS	0.260	0.157
	$-T\Delta S$ (at 300 K)	-78.0 (kcal/mol)	-47.1 (kcal/mol)

The last two rows give the total entropy change and corresponding energy change at room temperature upon desorption. All entropies are given in kcal/mol/K.

There is an error associated with these values that unfortunately is very hard to estimate from a QH analysis. Fig. 6 shows that S_{QH} looks converged, but it is possible that extending the simulations would make the values change significantly as more parts of the phase space is sampled. The discussion must therefore take place on a qualitative and semi-quantitative level.

One interesting conclusion from this calculation is that the change in entropy upon desorption corresponds to energy contributions that are large, -47 kcal/mol for the modified fragment and -78 kcal/mol for the native one, at room temperature. These values are larger in magnitude than the calculated free energy change ΔG. As noted above, the free energy change is to a large extent accounted for by change in potential energy. For this reason, the configurational entropy contribution must be canceled by an equally large term, which also has to be of entropic origin. The conclusion is that this term is ΔS_{SOL} mentioned above. By removing the XG fragment from the MTM surface, more surface area, of both MTM and XG, is exposed to water. Since structuring of water at a macromolecular interface leads to a decrease in entropy [27] this makes sense, at least intuitively. To really quantify to which extent the water and the counter ions contribute to ΔG is non-trivial and is outside the scope of the present work.

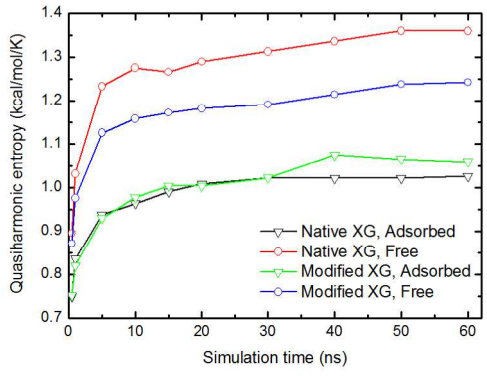

Figure 6. Time development of the calculated quasiharmonic entropy from four trajectories representing the free and the adsorbed state of native XG and modified XG, respectively.

3.4 Structural properties of adsorbed and free XGs

The most important structural parameters of XG are the three torsional angles Φ, Ψ and ω (Fig. 1). These torsions were therefore used to monitor conformational changes during the simulations. To avoid effects from end residues, only glycosidic linkages and side chain dihedrals from the middle part of each fragment were inspected, i.e., Φ and Ψ in G3, G4, G5 and G6, and ω2, ω3, ω4 and ω5. Only the B [180°] systems were included in the analysis considering the strongest interaction for both native and modified XG with MTM clays. The results are given in Table 4.

It is interesting to see that the adsorbed XG fragments became linear-like. In contrast to the results of XG adsorbed on cellulose [9], the analysis showed that it is more favorable for the backbone to adsorb on the MTM surface than for the side chains (see Fig. 8). This was validated by the dihedrals listed in Table 4. Since (Φ, Ψ) = (29°, –30°) represents a 'flat' linkage between two glucosyl residues and (Φ, Ψ) = (56°, 3°) reflects a 'twisted' one [10], Table 4 shows that all the glycosidic linkages of the native XG are 'flat'. In the modified XG, half of the linkages were 'flat' (marked as bold), and the other half were 'twisted'. This result indicates that when the galactosyl residue of the native XG was removed, the flat conformation became less favorable.

The dihedral angles ω further reflected the branching chain conformations of the XGs. Generally, there are three stable staggered rotamers, *gg* (gauche-gauche), *gt* (gauche-trans) and *tg* (trans-gauche) characterized by the O_6-C_6-C_5-O_5 dihedral angle, corresponding to ω~-60°, ω~60° and ω~180°, respectively (See Fig. 7).[28] In the lowest energy conformations found in this study, the native XG fragment has two torsions in *gg* (ω2 and ω5), and two in *gt* (ω3 and ω4), while the modified fragment has more *gg* (ω2, ω3 and ω5) than *gt* (see Table 4).

The gauche effect is defined as an internal stereoelectronic or hyperconjugative property in a fragment like X-C-C-Y, where X and Y represent electronegative atoms, and is akin to the description of the anomeric effect.[29-31] This effect is difficult to quantify,[28] but to some extent, the population of *gg, gt* and *tg* may reflect the stability of XG in aqueous solution. In other words, the more *gauche* orientations, the bigger the energy barrier, and the more flexible the structure becomes. As can be seen from Table 4 and Fig. 8, the ω3 values for the two XGs are typically different (marked in bold). As suggested in Fig. 7, we speculate that the *gt* conformation (the less gauche orientation), as opposed to *gg*, favors extended disaccharide and trisaccharide side chains, which lead to a shorter distance (0.1nm shorter than modified one) between backbone and MTM and accordingly could explain why the native XG show stronger adsorption than the modified one. And the similar phenomenon was previously found in XG adsorption on cellulose as well.[9]

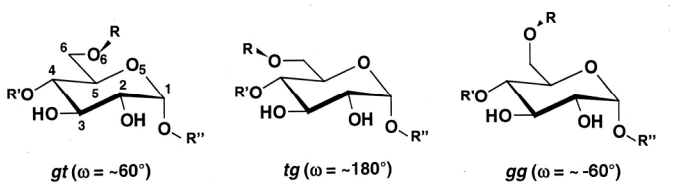

Figure 7. Definitions of the *gt*, *tg* and *gg* conformations with regard to the side chain orientations.

Table 4. Glycosidic linkages and side chain dihedral angles (°) for the adsorbed lowest energy XG fragments (native XG with B[180°] orientation and modified XG with B[180°] orientation). Data is averaged over the last 20 ns of the 100 ns trajectories.

Glycosidic linkage	Native XG		Modified XG		Side chain	Native XG		Modified XG	
	Φ	Ψ	Φ	Ψ					
G3	30.1±7.9	-23.2±10.5	40.2±7.6	19.0±11.5	ω2	-68.7±9.3	*gg*	-79.4±8.7	*gg*
G4	25.3±7.7	-31.4±8.7	44.5±9.0	-4.8±11.3	ω3	**70.9±11.4**	***gt***	**-76.7±9.6**	***gg***
G5	27.2±7.5	-28.1±8.9	**30.7±9.5**	**-19.9±9.7**	ω4	68.4±9.1	*gt*	68.7± 8.9	*gt*
G6	27.7±6.1	-33.6±9.5	**30.0±6.7**	**-32.8±8.7**	ω5	-67.7±11.0	*gg*	-62.4±9.2	*gg*

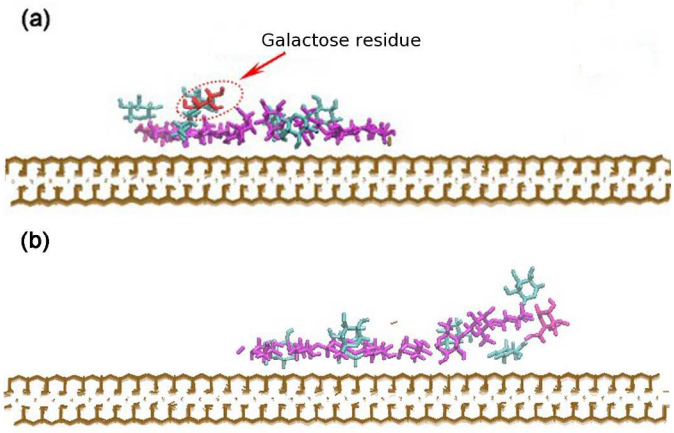

Figure 8. Snapshots of the adsorbed XG on MTM (B [180°], t=100 ns), Native XG, (a); Modified XG, (b). Water molecules and sodium ions are not shown for clarity. Color scheme is as follows: MTM residues (ochre), glucan backbone residues (magenta), side chain xylosyl residues (cyan), galactosyl residue (red).

The same dihedral angles were also analyzed for free XG fragments in water. Snapshots of the conformations after 60 ns are shown in SI Fig. S3. In the free-state case, all glycosidic linkages feature the "twisted" conformation, in both native and modified XG fragments, which clearly indicate that in the free state this conformation is favored over the "flat" conformation (see Table S1). Moreover, ω exhibits mostly the *gg* conformation, which suggests the more flexible structure found in the free state.

4 Conclusions

The present study clarifies the seemingly contradictory experimental observations of favorable mechanical integrity of the MTM-XG interface in hydrated nanocomposites[5], although XG is soluble in water. XG adsorbs to MTM in a flat conformation so that strong electrostatic and van der Waals interactions are formed. Indeed, a decomposition of the binding free energy into its enthalpic and entropic constituents reveals that the adsorption process is driven by enthalpy, which in this case is potential energy.

The adsorption of XG to MTM is associated with a penalty in entropy. Although this penalty is significant, as revealed by a quasi-harmonic analysis, it is apparently not large enough to overcome the gain in entropy as water and counter ions present at the MTM surface are liberated. In fact, since the whole free energy difference can be accounted for by the potential energy, these contributions have to be equal in magnitude, but of opposite sign.

The strong physical adsorption of the XGs to clay indicated from experimental data is confirmed by substantial wet work of adhesion estimates of around 0.6-0.7 J/m^2. The estimate is based on calculations of desorption free energy. In experiments, galactose side groups of native XG have been enzymatically removed. In the simulations, the native XG fragment exhibits a stronger binding affinity of 27 kcal/mol versus 23 kcal/mol for enzymatically modified XG. This is in qualitative agreement with experimental observations.

The presence of galactose side groups in native XG facilitates interfacial interaction with MTM. Analysis of conformational properties indicates that the reason is that galactose affects the conformation of the glucan backbone so that it becomes more flat in native XG. Furthermore, the side chain torsion angles in native XG exhibit more *gt* conformations than in modified XG, implicates the stronger adsorption.

These insights are helpful to future efforts on selection and molecular tailoring of complex polysaccharide structures for moisture stable clay-polysaccharide nanocomposites. For instance, Molecular Dynamics simulations can be used to suggest new chemical and enzymatic modification efforts. Although not studied explicitly, it is also apparent that the nature of counter ions present at the clay/polymer interface is important for wet interfacial adhesion.

Acknowledgements

Computations were performed on resources provided by the Swedish National Infrastructure for Computing (SNIC) at PDC Centre for High Performance Computing (PDC-HPC) by the project "Modeling of molecular interaction between nanoparticles and polymeric molecules", SNIC 025/12-38. Molecular graphics were produced using VMD.[32] Thanks to Li Xin and Qiong Zhang for helping conducting the modeling work and for providing initial data. Thanks also to Joby Kochumalayil for disclosing QCM data prior to publication. Partial funding from VR 2013-4058 and SSF FireFoam for JW is gratefully acknowledged.

Notes and references

[a] *Division of Theoretical Chemistry and Biology, School of Biotechnology, KTH Royal Institute of Technology, SE-106 91 Stockholm, Sweden*

[b] *Department of Fibre and Polymer Technology, School of Chemical Science and Engineering, SE-100 44 Stockholm, Sweden*

[c] *Wallenberg Wood Science Centre, KTH Royal Institute of Technology, SE-100 44 Stockholm, Sweden*

† Electronic Supplementary Information (ESI) available: Molecular dynamics simulation details, the in-depth descriptions of the methods used to estimate the equilibrated state, evaluating the binding affinity, and calculating the quasiharmonic entropy. It also presents interaction energy change and RMSDs for the quasi-equilibrated adsorbed state estimation

of all the initial 8 XG segment orientations (Fig. S1 and Fig. S2). The conformational properties of the free state XGs are presented in Table S1. The corresponding snapshots are shown in Fig. S3. See DOI: 10.1039/b000000x/

1 P. Fratzl, H. S. Gupta, F. D. Fischer and O. Kolednik, *Adv. Mater.*, 2007, **19**, 2657-2661.
2 M. Abdelmouleh, S. Boufi, M. N. Belgacem, A. Dufresne and A. Gandini, *J. Appl. Polym. Sci.*, 2005, **98**, 974-984.
3 P. Fratzl and R. Weinkamer, *Prog. Mater. Sci.*, 2007, **52**, 1263-1334.
4 Z. Tang, N. A. Kotov, S. Magonov and B. Ozturk, *Nat. Mater.*, 2003, **2**, 413-418.
5 J. J. Kochumalayil, M. Bergenstråhle-Wohlert, S. Utsel, L. Wågberg, Q. Zhou and L. A. Berglund, *Biomacromolecules*, 2013, **14**, 84-91.
6 J. J. Kochumalayil, S. Morimune, T. Nishino, O. Ikkala, A. Walther, and L. A. Berglund, *Biomacromolecules*, 2013, **14**, 3842-3849.
7 J. J. Kochumalayil, H. Sehaqui, Q. Zhou and L. A. Berglund, *J. Mater. Chem.*, 2010, **20**, 4321-4327.
8 M. Lopez, S. Fort, H. Bizot, A. Buléon and H. Driguez, *Carbohyd. Polym.*, 2012, **88**, 185-193.
9 Q. Zhang, H. Brumer, H. Ågren and Y. Tu, *Carbohydr. Res.*, 2011, **346**, 2595-2602.
10 S. Levy, W. S. York, R. Stuike-Prill, B. Meyer and L. A. Staehelin, *Plant J.*, 1991, **1**, 195-215.
11 C. E. A. F. Schafmeister, W. S. Ross and V. Romanovski, *LEAP*, University of California, San Francisco, 1995.
12 A. Plancon, *Clay Miner.*, 2001, **36**, 1-14.
13 J. H. Lee and S. Guggenheim, *Am. Mineral.*, 1981, **66**, 350-357.
14 R. T. Cygan, J. J. Liang and A. G. Kalinichev, *J. Physical Chem. B*, 2004, **108**, 1255-1266.
15 D. van der Spoel, E. Lindahl, B. Hess, G. Groenhof, A. E. Mark and H. J. C. Berendsen, *J. Comput. Chem.*, 2005, **26**, 1701-1718.
16 D. van der Spoel, E. Lindahl, B. Hess, A. R. van Buuren, E. Apol, P. J. Meulenhoff, D. P. Tieleman, A. L. T. M. Sijbers, K. A. Feenstra, R. van Drunen and H. J. C. Berendsen, Gromacs User Manual version 4.5.4, www.gromacs.org (2010)
17 K. N. Kirschner, A. B. Yongye, S. M. Tschampel, J. González-Outeiriño, C. R. Daniels, B. L. Foley and R. J. Woods, *J. Comput. Chem.*, 2008, **29**, 622-655.
18 M. A. Thyveetil, P. V. Coveney, H. C. Greenwell and J. L. Suter, *J. Am. Chem. Soc.*, 2008, **130**, 4742-4756.
19 H. J. C. Berendsen, J. P. M. Postma, W. F. van Gunsteren and J. Hermans, *Intermol. Forces*, 1981, 331-342.
20 J. Kästner, *Wiley Interdiscip. Rev.: Comput. Mol. Sci.*, 2011, **1**, 932-942.
21 M. Karplus and J. N. Kushick, *Macromolecules*, 1981, **14**, 325-332.
22 R. Baron, W. F. van Gunsteren and P. H. Hünenberger, *Trends Phys. Chem.*, 2006, **11**, 87-122.
23 K. N. Kirschner and R. J. Woods, *Proc. Natl. Acad. Sci.*, 2001, **98**, 10541-10545.
24 B. M. Pinto and R. Y. N. Leung, *The Anomeric Effect and Associated Stereoelectronic Effects*, Americal Chemistry Society, Washington, DC, 1993.
25 N. D. Epiotis, S. Sarkanen, D. Bjorkquist, L. Bjorkquist and R. Yates, *J. Am. Chem. Soc.*, 1974, **96**, 4075-4084.
26 N. K. de Vries, H. M. Buck., *Carbohydr. Res.*, 1987.
27 K. Kendall, *Molecular Adhesion and Its Applications: The Sticky Universe*, Kluwer Academic/Plenum, New York, 2001.
28 R. Baron, P. H. Hu□nenberger and J. A. McCammon, *J. Chem. Theory Comput.*, 2009, **5**, 3150-3160.
29 L. Perić-Hassler, H. S. Hansen, R. Baron and P. H. Hünenberger, *Carbohydr. Res.*, 2010, **345**, 1781-1801.
30 C. S. Pereira, D. Kony, R. Baron, M. Müller, W. F. van Gunsteren and P. H. Hünenberger, *Biophys. J.*, 2006, **90**, 4337-4344.
31 D. Chandler, *Nature*, 2005, **437**, 8.
32 D. A. Humphrey W and Schulten K., *J. Mol. Graphics*, 1996, **14**, 33-38.

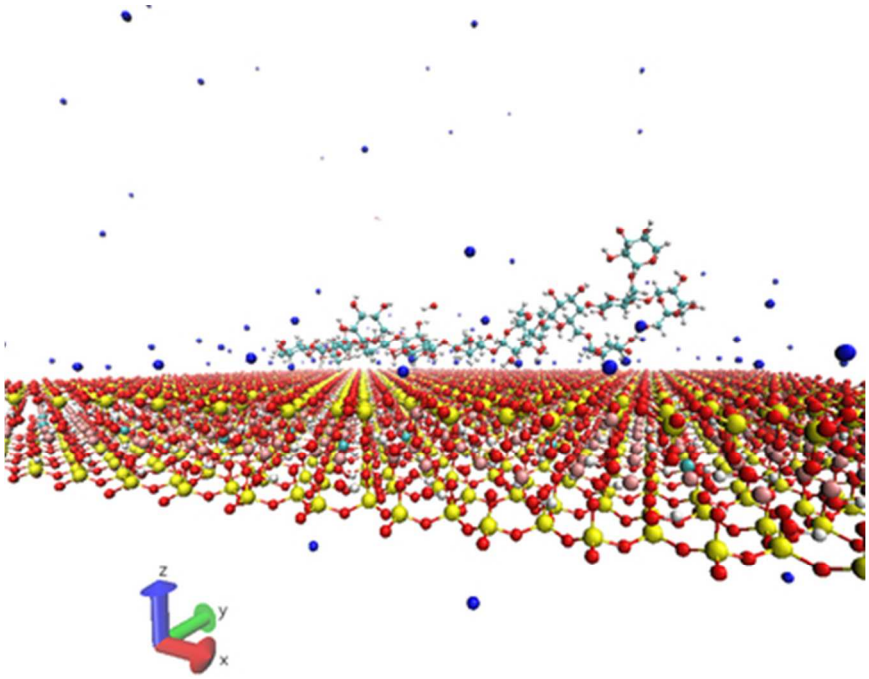

The thermodynamics of xyloglucan adsorption to montmorillonite clay in water was studied with molecular dynamics simulations
36x33mm (300 x 300 DPI)